Inorg. Chem. **2004**, *43*, 6479–6489

Mechanism of H_2O_2 Dismutation Catalyzed by a New Catalase Mimic (a Non-Heme Dibenzotetraaza[14]annulene–Fe(III) Complex): A Density Functional Theory Investigation

Xin Wang, Shuhua Li,* and Yuansheng Jiang

Department of Chemistry, Institute of Theoretical and Computational Chemistry, Laboratory of Mesoscopic Chemistry, Nanjing University, Nanjing, 210093, P. R. China

Received March 4, 2004

The mechanism of H_2O_2 dismutation catalyzed by the dibenzotetraaza[14]annulene–Fe(III) complex ($[Fe(C_{24}H_{22}N_4O_4)]^+$) which was recently reported (Paschke, J.; Kirsch, M.; Korth, H. G.; de Groot, H.; Sustmann, R. *J. Am. Chem. Soc.* **2001**, *123*, 11099) has been investigated by density functional theory using the B3LYP hybrid functional. The quartet potential energy profile of the catalytic reaction has been explored. In the whole catalytic cycle, the rate-determining step is found to be the O–O bond homolytic cleavage, without the assistance of solvent molecules in the second coordination shell. The calculated free energy barrier for this step is 10.8 kcal/mol, which is in reasonable agreement with the experimental facts. The calculations also show that the hydroxyl and hydroperoxyl radicals may be generated in the reaction processes, but they can be efficiently quenched in strongly exothermic steps. This study provides a satisfactory explanation to the observed efficiency of the H_2O_2 dismutation catalyzed by this complex.

1. Introduction

Hydrogen peroxide is a ubiquitous metabolite in living cells.[1] Excess hydrogen peroxide may oxidize cellular components.[2] Thus, it is very important for cells to remove the hydrogen peroxide. To protect the cells from the toxic effects by H_2O_2, nature has developed many different enzymatic systems. Among them, catalase is a very highly effective species, which can catalyze the decomposition of hydrogen peroxide into oxygen and water as in the following:

$$2H_2O_2 \xrightarrow{\text{catalase}} O_2 + 2H_2O \qquad (1)$$

Catalases are commonly classified into three classes in prokaryotes: (i) heme catalases; (ii) catalase−peroxidases; (iii) manganese catalases.[3] In fact, peroxidases are different from heme catalases and manganese catalases in that they catalyze the reduction of hydrogen peroxide to water but without oxygen evolution.[4] Catalase−peroxidases are bifunctional enzymes that exhibit both catalase and peroxidase activity.[3] Manganese catalases have an active site with a bridged binuclear mangnese cluster.[5] Catalase−peroxidases and heme catalases have similar active sites, which consist of a iron(III) core coordinated by a porphyrin and a protein residue, depending on the type of catalase−peroxidases and heme catalases. In catalase−peroxidases, like in most peroxidases, the axial ligand of the iron is a histidine, while, in heme catalases, this ligand is a unique tyrosine.[3] Among the three types of catalases, only heme catalases have been described for higher organisms.[6,7]

It is very important and interesting to know how heme catalases act in H_2O_2 dismutation reactions. There have been extensive studies on the mechanism of H_2O_2 dismutation reaction catalyzed by heme catalases. A commonly accepted mechanism[6,8−11] involves two steps: (i) The resting iron(III) in heme catalases is oxidized to an oxyferryl ($Fe^{IV}O$) state

* Author to whom correspondence should be addressed. E-mail: shuhua@netra.nju.edu.cn.

(1) Penninckx, M. J.; Elskens, M. T. *Adv. Microb. Physiol.* **1993**, *34*, 239.
(2) Halliwell B.; Gutteridge J. M. C. *Free Radicals in Biology and Medicine*, 2nd ed.; Clarendon Press: Oxford, U.K., 1993; pp 1−21.
(3) Zámocký, M.; Koller, F. *Prog. Biophys. Mol. Biol.* **1999**, *72*, 19.
(4) Everse, J.; Everse, K. E.; Grisham, M. B. *Peroxidase in Chemistry and Biology*; CRC Press: Boca Raton, FL, 1991; Vol. II.
(5) Barynin, V. V.; Vagin, A. A.; Melik-Adamyan, V. R.; Grebenko, A. I.; Khangulov, S. V.; Popov, A. N.; Andrianova, M. E.; Vainshtein, B. K. *Sov. Phys. Crystallogr.* **1986**, *31*, 457.
(6) Schonbaum, G. R.; Chance, B. In *The Enzymes*; Academic Press: New York, 1976; Vol. 13, p 363.
(7) Klotz, M. G.; Klassen, G. R.; Loewen, P. C. *Mol. Biol. Evol.* **1997**, *14*, 951.
(8) Chance, B.; Herbert, D. *Biochem. J.* **1950**, *46*, 402.

10.1021/ic049715j CCC: $27.50
Published on Web 09/04/2004

by a H_2O_2, and the macrocycle component is simultaneously oxidized to a porphyrin π-cation radical (por$\bullet^+$), which yields the so-called compound I and a H_2O molecule. (ii) A second H_2O_2 is oxidized by compound I to generate a H_2O and O_2, and heme catalase is recovered. While, for peroxidases, the first step is the same as described above, in subsequent reactions compound I oxdizes organic substrates to form so-called compoud II, and one electron reduction of compoud II then regenerates the native enzyme.[12,13]

Though there are large amounts of experimental investigations on catalases, the details of the two steps are not completely understood yet.[14] To understand the reaction mechanisms by heme catalase,[14] manganese catalase,[15,16] and heme peroxidase,[17] some quantum chemistry and molecular dynamics calculations have been performed previously. Kalko et al.[14] have investigated the mechanisms of substrate recognition by catalases using a variety of molecular dynamics methods. The importance of channels connecting the heme group and the exterior of proteins was analyzed in their work. For heme peroxidases, Wirstam, Blomberg, and Siegbahn[17] have studied the mechanism of O−O bond cleavage using hybrid density functional theory (DFT). Their calculations suggested that the mechanism of the formation of compound I consists of three steps. First, hydrogen peroxide is bound to the active site. Second, the nearby histidine abstracts a proton from the peroxide. Then the proton is donated back from the histidine to the other oxygen of the peroxide, with a simultaneous O−O bond breaking to form water and compound I. The calculated barrier of 10.4 kcal/mol is in reasonable agreement with the experimental barrier of 6.5 kcal/mol. For manganese catalase,[15,16] a DFT study has revealed that the O−O bond is homolytically cleaved in a spin-forbidden process with a calculated barrier of 15 kcal/mol, which is a rate-limiting step in the entire cycle.

To probe the molecular mechanism of H_2O_2 dismutation by catalases, chemists have also synthesized a series of model complexes to mimic the catalytic reaction of catalases. A lot of catalase models have been reported to exhibit "catalase-like" activity.[18−25] Recently, Paschke et al.[25] reported a new

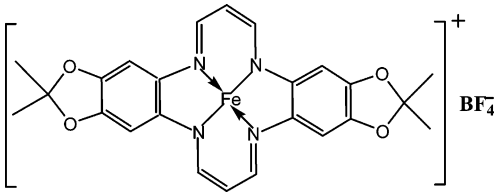

Figure 1. Structure of complex **1**.

catalase model, a non-heme dibenzotetraaza[14]annulene−Fe(III) ($[Fe(C_{24}H_{22}N_4O_4)]^+$; Ann−Fe(III) in short) complex (Figure 1). The structure of this complex was confirmed by analytical and spectroscopic data (its crystal structure was not available).[25] This catalase model was found to catalyze the H_2O_2 dismutation at micromolar concentrations, with the release of O_2 in high yield from low concentrations of H_2O_2 in phosphate buffer solution at pH = 7.2.[25] Compared to other non-porphyrin Fe(III) complexes reported before,[19−24] the Ann−Fe(III) complex is relatively effective in its catalase-like activity under physiological conditions. The reaction catalyzed by this complex is about 4000 times less efficient than that catalyzed by native catalases[25,26] but several orders of magnitude faster than that catalyzed by "free" ferrous ions in aqueous solution,[25,27] which is often called the Fenton reaction.[28] For the Fenton reaction, a widely accepted mechanism is that free hydroxyl radicals are the key intermediates.[29] However, increasing experimental evidence[30] has also suggested another alternative mechanism that a high-valent oxoferryl ($[Fe^{IV}O]^{2+}$) complex acts as the key intermediate. This mechanism is also supported from recent DFT calculations reported by Baerends's group.[31] With a hexa−aqua Fe^{II} complex as a catalyst, they showed that after the addition of H_2O_2 to the Fe(II) center the O−O bond is homolytically cleaved with a barrier of only 6 kcal/mol.[31a] Moreover, they found that the generated OH radical can be "trapped" in the complex to form a new water molecule, and the formation of the Fe(IV)−oxo intermediate is energetically favorable in water. Thus, ferrous ions in aqueous solution and ferric heme catalases (or peroxidases) catalyze the O−O bond cleavage in different ways but

(9) Nicholls, P.; Schonbaum, G. R. In *The Enzymes*; Academic Press: New York, 1963; Vol. 8, p 147.
(10) Deisseroth, A.; Dounce, A. *Physiol. Rev.* **1970**, *50*, 319.
(11) Maté, M. J.; Murshudov, G.; Bravo, J.; Melik-Adamyan, W.; Loewen, P. C.; Fita, I. In *Handbook of Metalloproteins*; Messerschmidt, A., Huber, R., Eds.; John Wiley: New York, 2001.
(12) Dunford, B. In *Heme Peroxidases*; Wiley-VCH: Weinheim, Germany, 1999; p 435.
(13) Akkara, J. A.; Wang, J.; Yang, D.; Gonsalves, K. *Macromolecules* **2000**, *33*, 2377.
(14) Kalko, S. G.; Gelpí, J. L.; Fita, I.; Orozco, M. *J. Am. Chem. Soc.* **2001**, *123*, 9665.
(15) Siegbahn, P. E. M. *Theor. Chem. Acc.* **2001**, *105*, 197.
(16) Siegbahn, P. E. M. *J. Comput. Chem.* **2001**, *22*, 1634.
(17) Wirstam, M.; Blomberg, M. R. A.; Siegbahn, P. E. M. *J. Am. Chem. Soc.* **1999**, *121*, 10178.
(18) Robert, A.; Loock, B.; Momenteau, M.; Meunier, B. *Inorg. Chem.* **1991**, *30*, 706.
(19) Melnyk, A. C.; Kildahl, N. K.; Rendina, A. R.; Busch, D. H. *J. Am. Chem. Soc.* **1979**, *101*, 3232.
(20) Zhang, X.-P.; Zhang, D.-L.; Busch, D. H.; van Eldik, R. *J. Chem. Soc., Dalton Trans.* **1999**, 2751.
(21) Okuno, T.; Ito, S.; Ohba, S.; Nishida, Y. *J. Chem. Soc., Dalton Trans.* **1997**, 3547.
(22) Than, R.; Schrodt, A.; Westerheide, L.; van Eldik, R.; Krebs, B. *Eur. J. Inorg. Chem.* **1999**, 1537.
(23) Ito, S.; Okuno, T.; Matsushima, H.; Tokii, T.; Nishida, Y. *J. Chem. Soc., Dalton Trans.* **1996**, 4479.
(24) Autzen, S.; Korth, H.-G.; Sustmann, R.; de Groot, H. *Eur. J. Org. Chem*. **2001**, 3119.
(25) Paschke, J.; Kirsch, M.; Korth, H. G.; de Groot, H.; Sustmann, R. *J. Am. Chem. Soc.* **2001**, *123*, 11099.
(26) Bergmeyer, J., Grassl, M., Eds. *Methods of Enzymatic Analysis*, 3rd ed.; Verlag Chemie: Weinheim, Germany, 1983; Vol. II, p 165.
(27) For rates of Fe(II)- and Fe(III)-catalyzed H_2O_2 decompositions see: Tachiev, G.; Roth, J. A.; Bowers, A. R. *Int. J. Chem. Kinet.* **2000**, *32*, 24 and references therein.
(28) (a) Fenton, H. J. H. *Chem. News* **1876**, 190. (b) Fenton, H. J. H. *J. Chem. Soc.* **1894**, *65*, 899.
(29) Haber, F.; Weiss, J. *Proc. R. Soc. London* **1934**, *147*, 332.
(30) (a) Bray, W. C.; Gorin, M. H. *J. Am. Chem. Soc.* **1932**, *54*, 2124. (b) Kremer, M. L. *Phys. Chem. Chem. Phys.* **1999**, *1*, 3595.
(31) (a) Buda, F.; Ensing, B.; Gribnau, M. C. M.; Baerends, E. J. *Chem.—Eur. J.* **2001**, *7*, 2775. (b) Ensing, B.; Buda, F.; Blöchl, P.; Baerends, E. J. *Angew. Chem., Int. Ed.* **2001**, *40*, 2893. (c) Ensing, B.; Buda, F.; Blöchl, P.; Baerends, E. J. *Phys. Chem. Chem. Phys.* **2002**, *4*, 3619. (d) Ensing, B.; Baerends, E. J. *J. Phys. Chem. A* **2002**, *106*, 7902. (e) Buda, F.; Ensing, B.; Gribnau, M. C. M.; Baerends, E. J. *Chem.—Eur. J.* **2003**, *9*, 3436.

generate the similar oxidizing intermediate (an oxoferryl species) for the subsequent step. The reaction of hydrogen peroxide with hexa−aqua iron(II) is somewhat relevant to that with iron(III) in heme-containing peroxidases and catalases.

To our knowledge, the mechanism of the reaction catalyzed by the Ann−Fe(III) complex is almost unknown. In this paper, we will use density functional theory (DFT) calculations to explore the potential energy profiles of H_2O_2 dismutation catalyzed by this Ann−Fe(III) complex. For larger systems containing transition metals such as metalloenzymes, hybrid density functional theory, especially B3LYP, has been established as the most useful theoretical tool for quantum chemistry calculations.[32] Although there are reports on the quantitative even qualitative failures of DFT in predicting activation barriers for some problematic cases,[33,34] in most cases studied so far the calculated B3LYP barriers are satisfactory in interpreting available experimental observations.[32] Thus, all our calculations will be carried out with B3LYP. Several alternative routes at different stages of the studied reaction will be investigated, and the results will be compared to each other and with related experimental and theoretical studies. Finally, a possible mechanism for the catalytic cycle of the studied reaction is suggested.

2. Computational Details

In all calculations, density functional theory (DFT) is employed with Becke's three-parameter nonlocal exchange functional[35] and the Lee, Yang, and Parr nonlocal correlation functional (B3LYP).[36] The relativistic effective core potential (ECP)[37] for iron is employed in all B3LYP calculations. The basis set for iron is a modified LANL2DZ double-ζ basis set plus an f-type polarization function,[38] in which the two 4p functions of the standard LANL2DZ have been replaced by the optimized 4p functions from Couty and Hall.[39] The standard 6-31G(d) basis set is employed for all Fe-bound nitrogen atoms and the substrate H_2O_2 (or oxygen and hydrogen atoms derived from it). For all the other atoms, the 6-31G basis set is used. All together, the basis set described above is called basis set I for simplicity. The geometries of reactants, intermediates, transition states, and products are fully optimized using the unrestricted B3LYP (UB3LYP) method with basis set I described above. For each species, the harmonic vibrational frequencies are calculated to obtain the zero point energies (ZPE) and verify whether it is a minimum or a transition state on the potential energy surfaces (PES). The temperature-dependent enthalpy corrections and the entropy effects are computed at 298 K and 1 atm of pressure. To take into account the solvent effects on the reaction, we perform single-point calculations on some species with the gas-phase-optimized geometries using a reaction field with the conductor-like screening solvation model (COSMO) method.[40] As the reaction happens in buffer solution, which contains only 0.2−1% DMSO, water is taken to be the solvent in calculations. In addition, the binding energies between van der Waals complexes are corrected for basis set superposition error (BSSE) using the Boys−Bernardi counterpoise method.[41]

To obtain more accurate energetics of potential energy profiles, we also perform single-point calculations with a larger basis set (basis set II). In basis set II, all Fe-bound nitrogen atoms and H_2O_2 are described with the 6-311++G(d,p) basis set and all the other atoms are described with the 6-31G(d) basis set. Unless stated specifically, the energies of all species discussed in the following sections are obtained with basis set II including the ZPE corrections obtained with basis set I. All calculations have been performed with the Gaussian 98 package of programs.[42]

3. Results and Discussion

3.1. Electronic Structure of the Model Catalyst. The model catalyst **1** used in our calculations is structurally almost identical with the experimental Ann−Fe(III) complex, except that four methyl groups being distant to the active site of the catalyst are replaced by four hydrogen atoms. The optimized structures of the model catalyst **1** at its lowest quartet and doublet states, ^{4}**1** and ^{2}**1**, are shown in Figure 2. In both ^{4}**1** and ^{2}**1**, the annulene macrocycle is nearly planar and symmetrical, and the four Fe−N bond lengths are almost the same. Thus, the catalyst **1** is a good delocalized system with D_{2h} symmetry, which is similar to the highly delocalized porphyrin ring in native catalases. Although in the literature there are some crystal structures and spectroscopic studies on a few five-coordinated and six-coordinated Ann−Fe(II) and Ann−Fe(III) complexes,[43] no crystal structures are available for four-coordinated Ann−Fe(III) complexes or their derivatives for direct comparison to the calculated results of ^{4}**1** and ^{2}**1**. To better judge the reliability of our calculations, we have performed calculations on a four-coordinated Ann−Fe(II) compound {(7,16-dihydro-6,8,15,-17-tetramethyldibenzo[*b,i*][1,4,8,11]tetraazacyclotetradecinato)-iron(II)}, whose crystal structure and spectroscopic information exist.[44] The optimized structure of this Ann−Fe(II) complex is in good agreement with the corresponding crystal structure

(32) (a) Siegbahn, P. E. M.; Blomberg, M. R. A. *Annu. Rev. Phys. Chem.* **1999**, *50*, 221. (b) Siegbahn, P. E. M.; Blomberg, M. R. A. *Chem. Rev.* **2000**, *100*, 421. (c) Himo, F.; Siegbahn, P. E. M. *Chem. Rev.* **2003**, *103*, 2421. (d) Siegbahn, P. E. M. *Faraday Discuss.* **2003**, *124*, 289. (e) Siegbahn, P. E. M. *Q. Rev. Biophys.* **2003**, *36*, 91.
(33) Zhang, Y.-K.; Yang, W.-T. *J. Chem. Phys.* **1998**, *109*, 2604.
(34) Patchkovskii, S.; Ziegler, T. *J. Chem. Phys.* **2002**, *116*, 7806.
(35) Becke, A. D. *J. Chem. Phys.* **1993**, *98*, 5648.
(36) Lee, C.; Yang, W.; Parr, R. G. *Phys. Rev.* **1988**, *B37*, 785.
(37) Hay, P. J.; Wadt, W. R. *J. Chem. Phys.* **1985**, *82*, 299.
(38) Ehler, A. W.; Böhme, M.; Dapprich, S.; Gobbi, A.; Höllwarth, A.; Jonas, V.; Köhler, K. F.; Segmann, R.; Velkamp, A.; Frenking, G. *Chem. Phys. Lett.* **1993**, *208*, 111.
(39) Couty, M.; Hall, M. B. *J. Comput. Chem.* **1996**, *17*, 1359.
(40) Barone, V.; Cossi, M. *J. Phys. Chem. A* **1998**, *102*, 1995.
(41) Boys, S. F.; Bernardi, F. *Mol. Phys.* **1970**, *19*, 553.
(42) Frisch, M. J.; Trucks, G. W.; Schlegel, H. B.; Scuseria, G. E.; Robb, M. A.; Cheeseman, J. R.; Zakrzewski, V. G.; Montgomery, J. A., Jr.; Stratmann, R. E.; Burant, C. J.; Dapprich, S.; Millam, J. M.; Daniels, A. D.; Kudin, K. N.; Strain, M. C.; Farkas, O.; Tomasi, J.; Barone, V.; Cossi, M.; Cammi, R.; Mennucci, B.; Pomelli, C.; Adamo, C.; Clifford, S.; Ochterski, J.; Petersson, A. G.; Ayala, Y. P.; Cui, Q.; Morokuma, K.; Malick, K. D.; Rabuck, D. A.; Raghavachari, K.; Foresman, B. J.; Cioslowski, J.; Ortiz, V. J.; Stefanov, B. B.; Liu, G.; Liashenko, A.; Piskorz, P.; Komaromi, I.; Gomperts, R.; Martin, L. R.; Fox, J. D.; Keith, T.; Al-Laham, A. M.; Peng, Y. C.; Nanayakkara, A.; Gonzalez, C.; Challacombe, M.; Gill, P. M. W.; Johnson, B.; Chen, W.; Wong, M. W.; Andres, J. L.; Gonzalez, C.; Head-Gordon, M.; Replogle, E. S.; Pople, J. A. *Gaussian 98*, revision A.11; Gaussian, Inc.: Pittsburgh, PA, 1998.
(43) (a) Nishida, Y.; Sumita, A.; Hayashida, K.; Ohshima, H.; Kida, S.; Maeda, Y. *J. Coord. Chem.* **1979**, *9*, 161. (b) Gottfried, V.; Weiss, A.; Dori, Z. *J. Am. Chem. Soc.* **1980**, *102*, 3946. (c) Deligeorgiev, T.; Mitewa, M.; Russanov, V. *Synth. React. Inorg. Met.-Org. Chem.* **1993**, *23*, 1229. (d) Käpplinger, I.; Keutel, H.; Jäger, E.-G. *Inorg. Chim. Acta* **1999**, *291*, 190. (f) Mountford, P. *Chem. Soc. Rev.* **1998**, *27*, 105.
(44) Goedken, V. L.; Pluth, J. J.; Peng, S.-M.; Bursten, B. *J. Am. Chem. Soc.* **1976**, *98*, 8014.

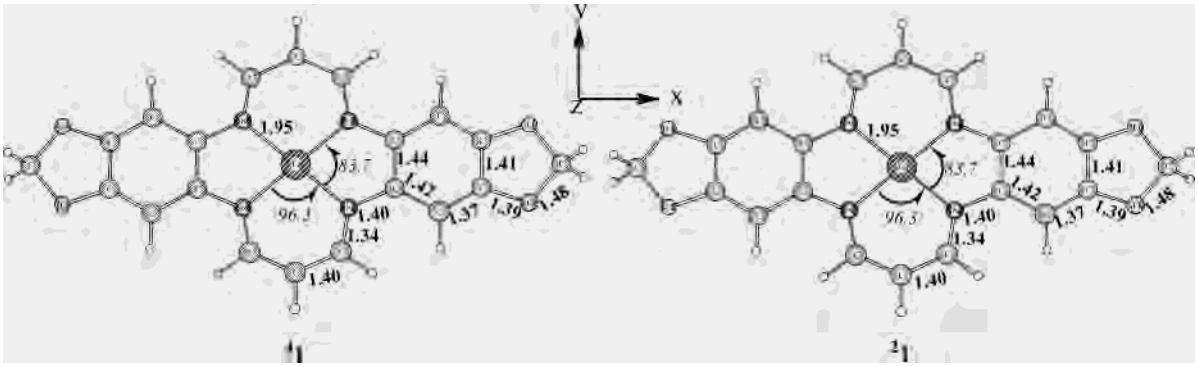

Figure 2. Optimized structures of the model catalyst **1** at its lowest doublet and quartet states, ^{4}**1** and ^{2}**1**. The bond distances are in Å, and bond angles, in deg.

Chart 1. Qualitative Molecular Orbital Picture Describing the Electronic Structures of ^{4}**1** and ^{2}**1**

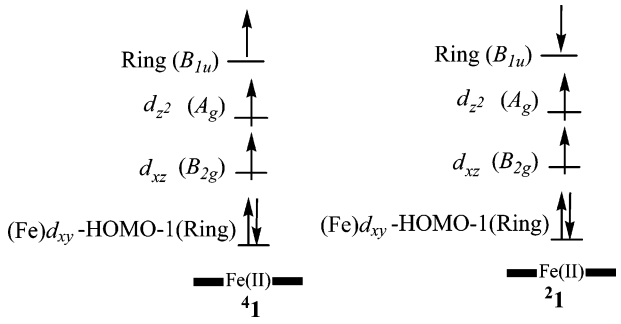

(see Figure S1 of the Supporting Information). The ground state of this species is calculated to be a triplet state with two unpaired electrons on iron, and its lowest singlet state is about 34 kcal/mol higher in energy than the triplet state. These results are also in accord with the related experimental facts.[44] Thus, one may expect that our calculations should give satisfactory descriptions on geometries and electronic structures of the Ann−Fe(III) catalyst and other related species under study.

Interestingly, ^{4}**1** and ^{2}**1** have identical electronic energies within 0.1 kcal/mol (see Tables S1 and S2 in the Supporting Information). For both electronic states, their singly occupied orbitals are illustrated in Chart 1. In both spin states, three orbitals for unpaired electrons consist of a B_{1u} orbital of the annulene ring, which is the HOMO of the whole system, and two 3d orbitals (d_{z^2} and d_{xz}) of iron. As one can see, an unpaired electron in the annulene macrocycle is coupled to two unpaired electrons on the iron center antiferromagnetically in ^{2}**1** but ferromagnetically in ^{4}**1**. The near degeneracy of both electronic states implies that the magnitude of spin coupling between the unpaired electron in ring and two unpaired electrons on iron is quite weak. The natural population analysis shows that, at the two spin states, the annulene ligand is already oxidized and the iron atom is actually in Fe(II). This result is in contrast to the similar porphyrin−Fe(III) complex, where the porphyrin ligand is not oxidized and the iron atom is in Fe(III).[45] The reason the annulene ligand can reduce Fe(III) to Fe(II) may be partly attributed to the fact that the anion of the annulene with the geometry as in ^{4}**1** and ^{2}**1** is about 49.4 kcal/mol more stable than the dianion of the annulene, while, for the porphyrin ligand in the porphyrin−Fe(III) complex, our calculations show that its anion is only 32.8 kcal/mol lower in energy than its dianion. As a result, the resting state of the tetraazaannulene ferric catalyst in fact consists of a ferrous iron plus a "cation-radical" ligand.

Considering the fact that the studied catalase model works in phosphate buffer solution at pH = 7.2, it is worth investigating whether the electronic structure of the model catalyst **1** is significantly affected by two water molecules axially coordinated to the iron. We have optimized the corresponding structures at both doublet and quartet states. These two structures (not shown) are also found to be nearly degenerate, and the charge and spin densities of these two species show that the spatial distributions of unpaired electrons are quite similar to those in ^{4}**1** and ^{2}**1**. In both spin states, we found that the energy required to dissociate an axial water to form a five-coordinated species (after BSSE corrections are included) is about 4.8 kcal/mol. Thus, it is easy to create an open coordination site, allowing for H_2O_2 to exchange with a water ligand. On the other hand, once an axial ligand is bound to the iron center (as in all stationary points studied hereafter), the loss of another water ligand would be facile. Therefore, for simplicity we neglect the axial ligation of a water molecule to the iron in all intermediates and transition states studied below.

3.2. Quartet Potential Energy Profile. For all species involved in the catalytic cycle, their lowest quartet and doublet states are found to have very close energies (as shown in Tables S1 and Table S2 of the Supporting Information). The bonding difference in both electronic states for all these species is very similar to that in ^{4}**1** and ^{2}**1**, i.e., an unpaired electron in the ring couples to unpaired electrons on the iron center antiferromagnetically in the doublet state but ferromagnetically in the quartet state. We notice that the calculated spin contamination is small for all quartet species but quite severe for all doublet species. This result indicates that the species at the doublet state have significant multireference character, while the corresponding quartet species do not. Since the current single-determinant DFT method is more reliable for electronic states with dominant single-reference character than for electronic states with significant multireference character, in the following only the results

(45) Oliveira, K. M. T.; Trsic, M. *J. Mol. Struct. (THEOCHEM)* **2001**, *539*, 107.

Chart 2. Possible Pathways of the Reaction in Stages 1 and 2

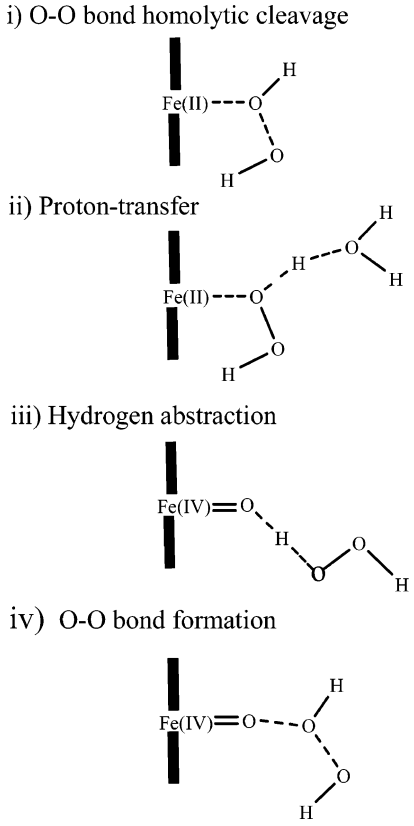

obtained for the quartet species are reported and discussed. Although restricted ensemble-referenced KS-DFT (REKS)[46] or CAS-DFT[47] methods have been developed for tackling multireference electronic states, they are still computationally prohibitive for large systems under study here.[46,47] The optimized structures for all doublet species and the doublet potential energy profile are shown in Figures S5, S3, and S4 of the Supporting Information.

The mechanism of the whole reaction can be assumed to be similar to the proposed mechanism of the reaction catalyzed by catalases[6,8−11] and by ferrous ions from recent theoretical studies.[31a,31e] According to this assumption, the whole catalytic cycle can be divided into two stages, as shown in the following:

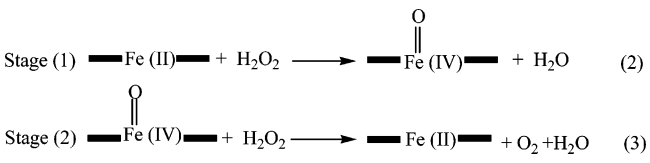

In stage 1, the catalyst **1** is oxidized by H_2O_2 to become the oxoferryl complex, generating a H_2O molecule. In stage 2, the oxoferryl species oxidizes the second H_2O_2 and accepts two electrons to recover the resting form, yielding a H_2O and O_2. As shown in Chart 2, in stage 1 there are two possible pathways for the first step: the O−O bond homolytic cleavage and the proton-transfer with the assistance of an additional H_2O in the second coordination shell. In stage 2, the reaction also may start toward two different directions: hydrogen abstraction and O−O bond formation. Our calculations showed that in stage 1 the O−O bond homolytic cleavage is more energetically favorable than the proton-transfer pathway, while in stage 2 the hydrogen abstraction pathway is preferred. For compactness, the results of two energetically favorable pathways will be discussed first, and then the other two pathways will be compared and discussed briefly.

The quartet potential energy profiles of stages 1 and 2 are shown in Figures 3 and 4, respectively. The optimized geometries of intermediates, transition states, and products are displayed in Figure 5.

Hereafter we will discuss the potential energy profiles using the ZPE-corrected relative energies. In stage 1, initially, the catalyst ^{4}**1** attracts a H_2O_2 molecule to form an $Fe^{II}(H_2O_2)$ complex ^{4}**2**, which is 13.1 kcal/mol below the isolated ^{4}**1** and H_2O_2 molecule. As the oxygen atom of H_2O_2 approaches the iron center, the O−O bond of the complex ^{4}**2** is broken directly to form an intermediate Fe^{III}(OH···OH) complex ^{4}**4** through a transition state ^{4}**3ts**. This step is an O−O bond homolytic cleavage step with an activation barrier of 10.3 kcal/mol. The intermediate ^{4}**4** can release the weakly bound hydroxyl radical to generate an Fe^{III}(OH) intermediate ^{3}**5** and a hydroxyl radical. The free hydroxyl radical can attract the hydroxyl ligand of ^{3}**5** by adjusting its orientation to form a new Fe^{III}(OH···OH) complex ^{4}**6**, which is 3.6 kcal/mol lower in energy than ^{3}**5** and a hydroxyl radical. ^{4}**6** could convert into an Fe^{IV}(O···H_2O) complex ^{4}**8** through a hydrogen atom transfer transition state ^{4}**7ts**. Without the ZPE correction, the barrier of ^{4}**6** → ^{4}**8** is 1.7 kcal/mol. But when the ZPE correction is included, the energy of ^{4}**7ts** is 0.2 kcal/mol lower than that of the ^{4}**6**. Thus, ^{4}**6** could readily convert into the Fe^{IV}(O···H_2O) species ^{4}**8**. This step is strongly exothermic by 26.1 kcal/mol. Therefore, the formed hydroxyl radical can be efficiently quenched. The last step of stage 1 is the dissociation of the weakly coordinated H_2O from ^{4}**8** to form an oxoferryl species ^{4}**9**, which is endothermic by 6.4 kcal/mol. The overall process of stage 1 is exothermic by about 32.2 kcal/mol.

In stage 2, first, a second H_2O_2 is added to ^{4}**9** to form an Fe^{IV}(O···H_2O_2) complex ^{4}**10** with a energy lowering of 8.5 kcal/mol. By a hydrogen atom transfer, an Fe^{III}(OH···O_2H) intermediate ^{4}**12** is formed from ^{4}**10** through a transition state ^{4}**11ts** with a barrier of 9.7 kcal/mol. ^{4}**12** can release a hydroperoxyl radical to form an Fe^{III}(OH) species ^{3}**13** with a energy increase of 3.4 kcal/mol. Then, the free hydroperoxyly radical interacts with the oxygen of ^{3}**13** from another orientation to yield a new Fe^{III}(OH···O_2H) complex ^{4}**14,** which is 8.8 kcal/mol more stable than ^{4}**12**. Next, the hydrogen atom of the hydroperoxyly group could transfer to the hydroxyl ligand to generate an Fe^{II}(H_2O···O_2) complex ^{4}**16** through a transition state ^{4}**15ts**. This hygrogen atom transfer step is a low barrier but strongly exothermic process. Since for the Fe^{II}(H_2O···O_2) complex, its ground state is a sextet state ^{6}**16**, which is 9.1 kcal/mol lower in energy than

(46) (a)Filatov, M.; Shaik, S. *Chem. Phys. Lett.* **1999**, *304*, 429. (b) Filatov, M.; Shaik, S. C*hem. Phys. Lett.* **2000**, *332*, 409. (c) Filatov, M.; Shaik, S. *J. Phys. Chem. A* **2000**, *104*, 6628.
(47) Gräfenstein, J.; Cremer, D. *Chem. Phys. Lett.* **2000**, *316*, 569.

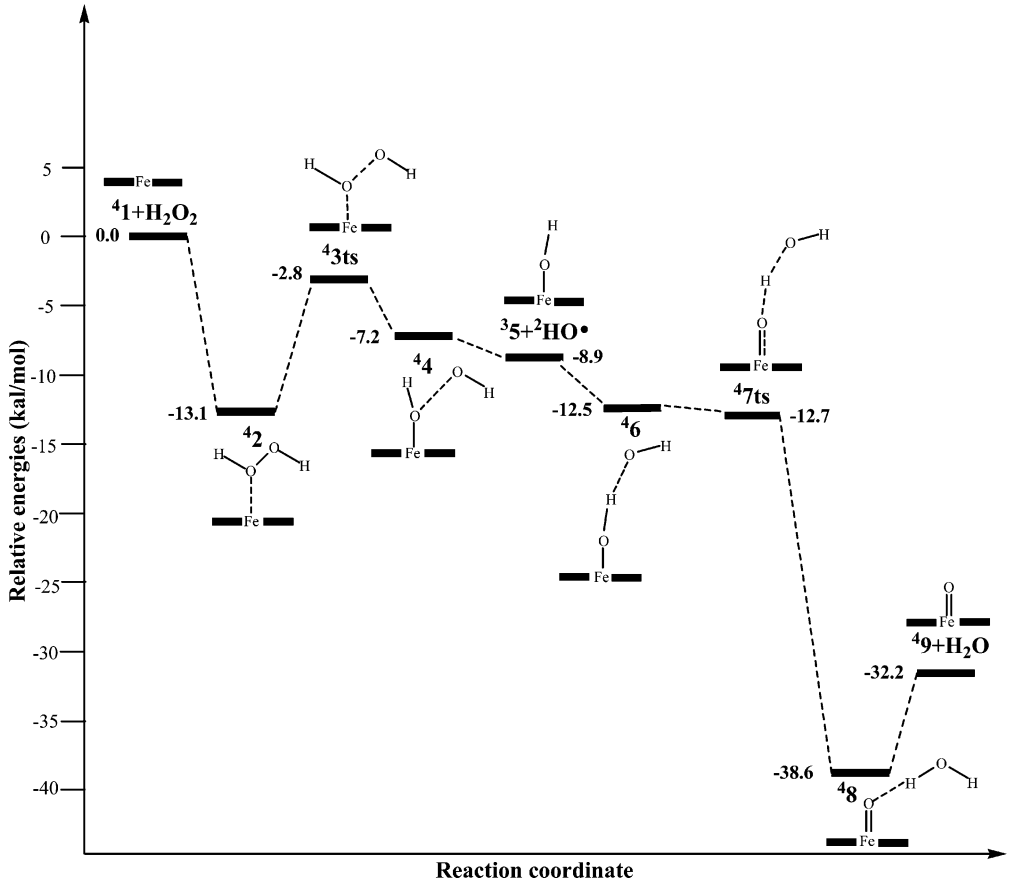

Figure 3. Quartet potential energy profile of stage 1. The ZPE corrections calculated with basis set I are included in the relative energies. The ZPE-corrected energy of ^{4}**1** + H_2O_2 is taken to be zero, which is −1565.022 23 au.

^{4}**16**, ^{4}**16** could convert into ^{6}**16** by surface crossing, which has the spin population similar to that in catalyst ^{4}**1**. Finally, a H_2O molecule and a ground-state O_2 are dissociated from ^{6}**16** to regenerate the catalyst ^{4}**1**. The whole process of stage 2 is exothermic by about 24.0 kcal/mol.

As mentioned above, the first step of stage 1 may also be the transfer of the hydrogen atom of H_2O_2 to an additional H_2O in the second coordination shell. First, the optimized structure of the $Fe^{II}(H_2O_2\cdots H_2O)$ complex ^{4}**17**, as showed in Figure 5, suggests that H_2O is strongly hydrogen-bonded to the $Fe^{II}(H_2O_2)$ complex ^{4}**2**. However, we failed to locate a stable intermediate with a proton transferred from the Fe-bound oxygen to H_2O. When optimizing the structure of this intermediate, we find that in a few steps the proton jumps back to the OOH ligand. By fixing the O3−H2 bond distance to 0.988 Å in free H_3O^+ and the bond angle of O1−H2−O3 to 171.4° in ^{4}**17** and optimizing all the other degrees of freedom, we see the resultant structure of the $Fe^{II}(OOH^-\cdots H_3O^+)$ species ^{4}**18** (in Figure 5) is 32.2 kcal/mol higher in energy than ^{4}**17**. Obviously, the energy required to promote this proton transfer is even higher than this value. Our preliminary calculations show that the addition of another water molecule in the second coordination shell may stabilize the hydronium ion H_3O^+ by 10.0 kcal/mol, but the corresponding proton transfer barrier is still at least 22.2 kcal/mol, significantly higher than the corresponding barrier along the O−O bond homolytic cleavage step. One may expect that adding more water molecules further stabilize the hydronium ion to some extent but has insignificant effect on decreasing the proton transfer barrier. Of course, in the discussions above we implicitly assume that under the experimental conditions (phosphate buffer solution at pH = 7.2) water exist primarily in the form of H_2O. If the hydroxide anion is present in the second coordination shell to accept a proton from the Fe-bound H_2O_2, the proton transfer pathway may be energetically favored. Since even at pH ∼ 7 hydroxide ions are still nonnegligible compared to the model compound, it is possible that the reaction of H_2O_2 with some model compounds may proceed through the proton-transfer pathway, as in peroxidases and catalases.[17] However, under the experimental conditions, the reaction is more likely to go though the O−O bond breaking pathway instead of the proton-transfer pathway. We notice that the same situation occurs for H_2O_2 to attack the hexa−aqua Fe^{II} catalyst.[31a]

To investigate whether the first step of stage 2 would proceed along the O−O bond formation pathway, we find a transition state for this O−O bond formation, ^{4}**19ts** (in Figure 5). As seen from the structure of this transition state, the O−O bond of H_2O_2 is being broken and the new O−O bond between Fe-bound oxygen and an oxygen of H_2O_2 is being formed. The spin distributions of this species reveal that the O−O bond of H_2O_2 is homolytically broken. The energy of ^{4}**19ts** is 26.8 kcal/mol higher than the total energies of the free reactant $Fe^{IV}O$ species ^{4}**9** and H_2O_2. Clearly, this barrier is much higher than the barriers of all steps along the

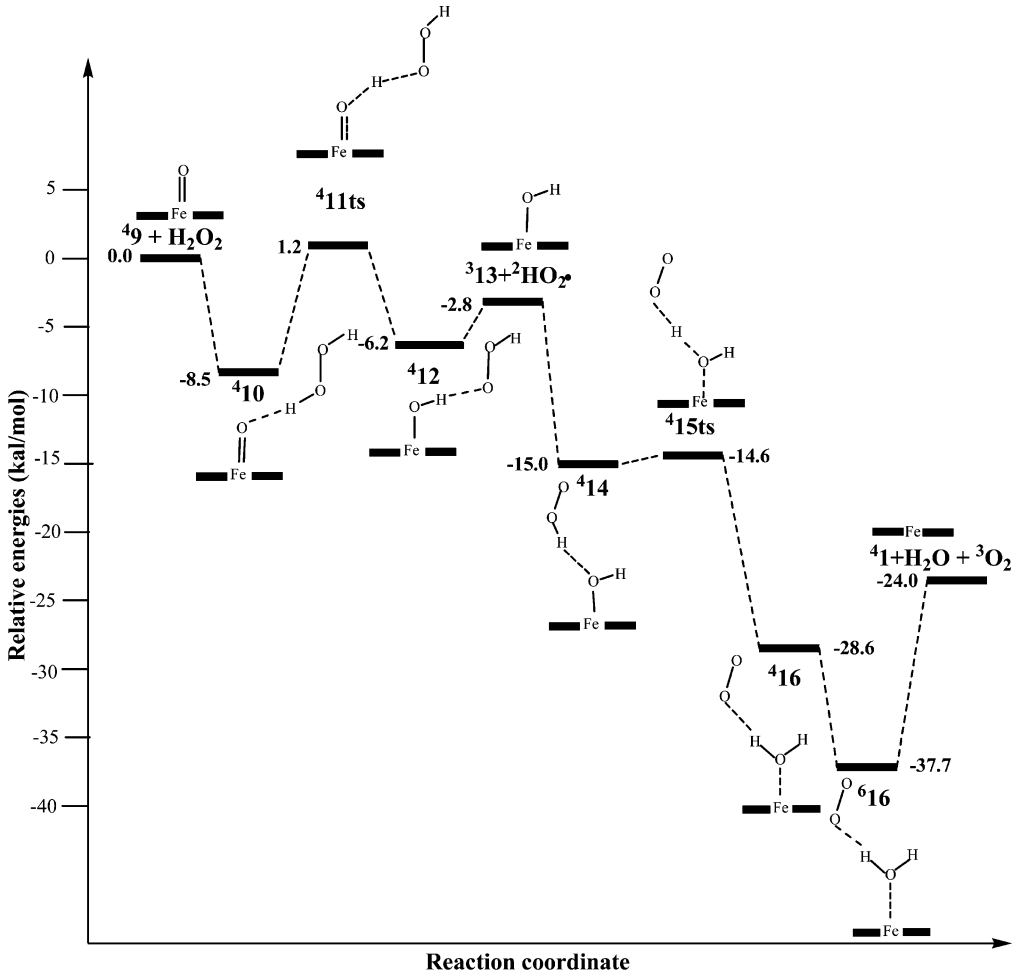

Figure 4. Quartet potential energy profile of stage 2. The ZPE corrections calculated with basis set I are included in the relative energies. The ZPE-corrected energy of **^{4}9** + H_2O_2 is taken to be zero, which is −1640.212 00 au.

hydrogen abstraction pathway, as described above. Therefore, the reaction of stage 2 would proceed through the hydrogen abstraction pathway instead of the O−O bond formation pathway.

To conclude from discussions above, the overall reaction may undergo the O−O homolytic cleavage pathway in stage 1 and the hydrogen abstraction pathway in stage 2. A combination of stages 1 and 2 shows that the overall reaction at the quartet pathway is strongly exothermic by 56.2 kcal/mol. The rate-limiting steps are the O−O bond cleavage in stage 1 and the dissociation of H_2O and O_2 from **^{6}16** in stage 2, respectively. The electronic energy barriers of these two steps are 10.3 and 13.7 kcal/mol, respectively. However, to get more reliable information on the rate-limiting steps, we have to rely on the calculated relative enthalpy and Gibbs free energies at 298 K for all species occurring on the quartet pathway, which are collected in Table 1. For the O−O bond cleavage step, the calculated Gibbs free energy barrier at 298 K is 10.8 kcal/mol, implying that the temperature and entropy effects are very small for the step. However, one can see from Table 1 that the entropy term plays a very important role in the dissociation steps of H_2O. For example, a large entropy effect makes the dissociation of H_2O and O_2 from **^{6}16** to be facile. Similarly, the entropy effect could cause the facile dissociation of H_2O from **^{4}8** to form **^{4}9**. Thus, according to the calculated Gibbs free energy barriers, the O−O bond cleavage with a barrier of 10.8 kcal/mol at 298 K is the rate-determining step in the whole catalytic cycle on the quartet reaction pathway.

The effect of the bulk solvent on the barriers should be taken into account. If this is done, we obtain a little lower free energy barrier of 10.7 kcal/mol for the O−O bond-breaking step. For the other three hydrogen atom transfer steps **^{4}6** → **^{4}8**, **^{4}10** → **^{4}12**, and **^{4}14** → **^{4}16**, the solvent effect leads to the decrease of Gibbs free energy barriers by 2.1, 0.6, and 0.7 kcal/mol, respectively. This result shows that the bulk solvent effect on the barriers of various steps in the studied reaction is insignificant. However, one should remember that if the reaction is in aqueous solution with different pHs the solvent may directly participate the reaction, like hydroxide ions described above.

Finally, although previous experiences[48] show that the B3LYP method is appropriate for studying the present reaction, it is also worthwhile to compare the performance of the B3LYP and CCSD(T) methods in studying some small molecules relevant to the key intermediates or transition states in the present reaction. The model systems chosen

(48) The discussions on the accuracy of the B3LYP method in studying some reactions similar to the present reaction are given on p S5 in the Supporting Information.

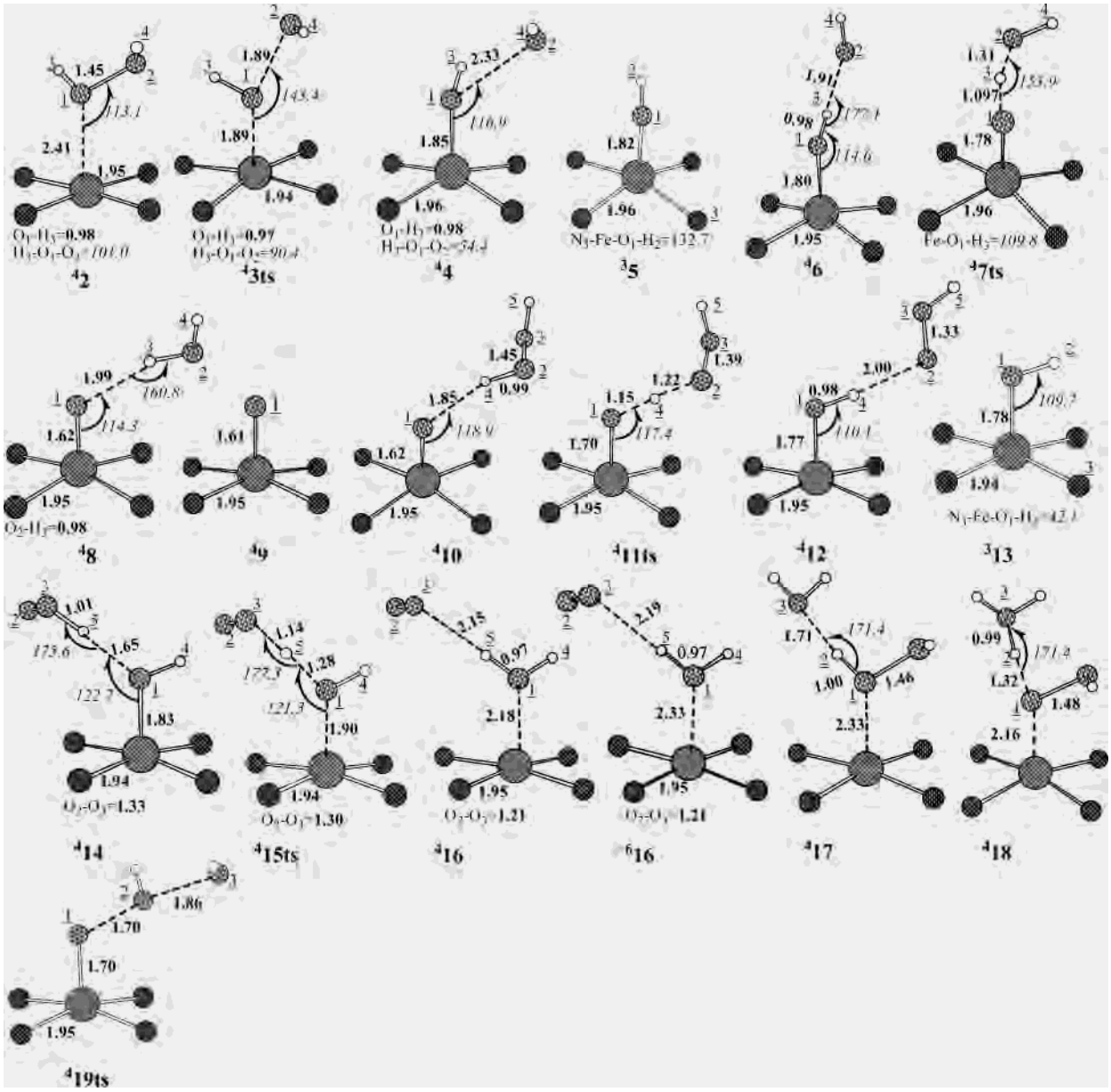

Figure 5. Optimized structures of intermediates and transition states along the quartet reaction pathway. The bond distances are in Å, and bond angles in deg. The annulene rings of all species are omitted for clarity. For all species, their geometries in Cartesian coordinates can be found in the Supporting Information. The Fe−N bond distance listed in the figure is the average of four Fe−N bond distances. In **^{4}18**, the O3−H2 bond distance is fixed to be 0.988 Å, which is the calculated O−H bond length in free H_3O^+, and the bond angle of O1−H2−O3 is fixed to be 171.4°, as in **^{4}17**.

Table 1. Calculated Relative Enthalpies[a] (kcal/mol) and Gibbs Free Energies (kcal/mol) for All Species at 298 K[b]

species	H_{298}	G_{298}	species	H_{298}	G_{298}
^{4}1 + $^1H_2O_2$	0.0	0.0	**^{4}9** + $^1H_2O_2$	0.0	0.0
^{4}2	−13.0	−3.3	^{4}10	−8.3	1.2
^{4}3ts	−2.9	7.5	^{4}11ts	0.6	10.8
^{4}4	−6.7	2.3	^{4}12	−5.6	1.1
^{3}5 + ^{2}HO•	8.1	−6.6	**^{3}13** + $^2HO_2$•	−2.7	−3.3
^{4}6	−11.8	−3.9	^{4}14	−14.9	−5.5
^{4}7ts	−12.8	−2.0	^{4}15ts	−14.7	−4.6
^{4}8	−38.4	−28.5	^{4}16	−27.5	−21.9
^{4}9 + ^1H_2O	−31.8	−30.6	^{6}16	−36.9	−30.1
			^{4}1 + ^1H_2O + $^3O_2$	−22.9	−33.9

[a] For stage 1, the enthalpy and Gibbs free energy of **^{4}1** + H_2O_2 are taken to be zero, respectively. For stage 2, those of **^{4}9** + H_2O_2 are taken to be zero. [b] The thermal corrections are calculated with basis set I. The corresponding electronic energies are obtained from the single-point calculations with basis set II.

to approximately represent species **^{4}2**, **^{4}3ts**, **^{4}6**, and **^{4}7ts** are $Fe^{2+}\cdots H_2O_2$, $Fe^{2+}\cdots OH\cdots OH$, $(FeOH\cdots OH)^{2+}$, and $(FeO\cdots H\cdots OH)^{2+}$, respectively. Their geometries are set to be the same as those of the corresponding fragments in optimized structures **^{4}2**, **^{4}3ts**, **^{4}6**, and **^{4}7ts**. More computational details are presented on p S5 in the Supporting

Scheme 1. Proposed Mechanism of H_2O_2 Dismutation Catalyzed by the Ann−Fe(III) Complex

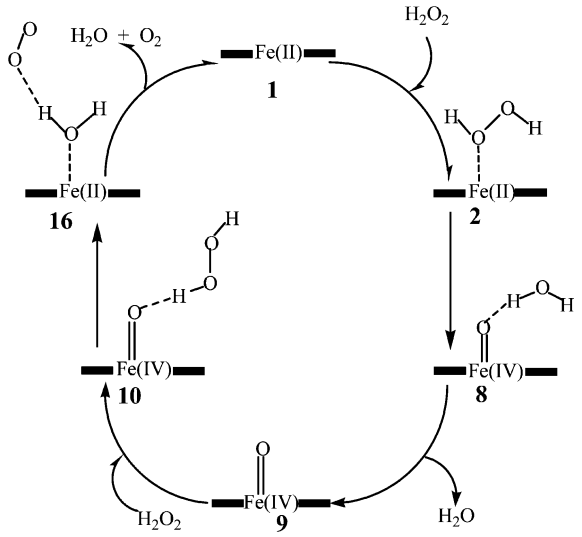

Information. Single-point calculations show that the energy difference between $Fe^{2+}\cdots H_2O_2$ and $Fe^{2+}\cdots OH\cdots OH$ calculated from B3LYP is smaller by 4.5 kcal/mol than that from CCSD(T). For two species $(FeOH\cdots OH)^{2+}$ and $(FeO\cdots H\cdots OH)^{2+}$, their energy difference obtained from B3LYP is only 0.6 kcal/mol below the corresponding CCSD(T) value. The closeness of the B3LYP and CCSD(T) energy differences may suggest that the accuracy of the B3LYP method for the O−O cleavage step (**^{4}2** → **^{4}3ts**) and the hydrogen atom transfer step (**^{4}6** → **^{4}7ts**) is satisfactory. Thus, one may expect that higher level calculations would not change the qualitative conclusions on the basis of this B3LYP study.

To summarize the discussions above, one can see that along the quartet pathway two H_2O_2 molecules can be readily converted into two H_2O molecules and one O_2 molecule by catalyst **1**. For the overall reaction, our proposed mechanism is shown in Scheme 1.

3.3. Optimized Geometries of Species along the Quartet Reaction Pathway. For all species from **^{4}2** to **^{4}16**, their annulene rings are also nearly planar. The bond lengths of rings are quite similar to those in **^{4}1**.

^{4}2 is an encounter complex of **^{4}1** and H_2O_2. The bond lengths of H_2O_2 in **^{4}2** are almost the same as those in free H_2O_2. In **^{4}3ts**, the Fe−O distance is shortened considerably and the O−O bond length is noticeably lengthened relative to those in **^{4}2**, indicating that the O−O bond is breaking. In the $Fe^{III}(OH\cdots OH)$ complex **^{4}4**, the distance between two oxygen atoms is 2.33 Å, implying that the O−O bond is almost broken. The hydrogen atoms bound to both oxygen atoms do not directly play a role in cleaving the O−O bond. Thus, this O−O bond-breaking picture is different from that in the proposed mechanism of H_2O_2 catalyzed by heme peroxidase.[17]

In the $Fe^{III}(OH\cdots OH)$ complex **^{4}6**, the hydroxyl radical is hydrogen-bonded to the Fe-bound hydroxyl ligand. The distance between O2 and H3 is 1.91 Å. From **^{4}6** to **^{4}8** through **^{4}7ts**, the distance between O1 and H3 increases from 0.98 to 1.99 Å, and the distance between O2 and H3 decreases from 1.91 to 0.98 Å.

Table 2. Spin Densities on Atoms of All Species and the Squared Magnitude of the Total Spin[a]

species	Fe	N	ring	O_1	O_2	O_3	$\langle S^2\rangle$
^{4}1	2.08	0.07	0.92				3.77
^{4}2	2.05	0.10	0.93	0.02	0.0		3.79
^{4}3ts	1.61	0.07	0.79	-0.06	0.66		3.93
^{4}4	2.55	0.10	1.02	0.29	−0.90		4.73
^{3}5	2.38	−0.10	−0.73	0.35			2.66
^{4}6	2.34	−0.09	−0.75	0.38	1.03		4.36
^{4}7ts	2.18	−0.05	−0.33	0.62	0.57		4.08
^{4}8	1.39	0.07	0.82	0.78	0.0		3.79
^{4}9	1.28	0.08	0.82	0.90			3.79
^{4}10	1.42	0.07	0.81	0.76	0.01	0.0	3.79
^{4}11ts	1.27	0.07	0.78	0.51	0.36	0.14	3.81
^{4}12	1.07	0.08	0.84	0.09	0.72	0.30	3.82
^{3}13	1.11	0.08	0.82	0.07			2.07
^{4}14	1.26	0.06	0.70	0.03	0.70	0.31	3.84
^{4}15ts	1.49	0.02	0.24	0.04	0.79	0.45	3.94
^{4}16	0.02	0.12	0.98	0.01	1.03	0.96	4.66
^{6}16	2.04	0.10	0.92	0.02	1.02	0.96	8.79
^{4}19ts	1.16	0.07	0.82	0.56	-0.21	0.69	3.88

[a] For the nitrogen atom, the value listed is the average of spin densities on four nitrogen atoms.

The $Fe^{IV}O$ species **^{4}9** is structurally similar to compound I in the enzymatic reaction. In **^{4}9**, the Fe−O bond length is about 1.61 Å, showing the double bond character. In the $Fe^{IV}(O\cdots H_2O_2)$ complex **^{4}10**, the hydrogen bond O1···H4−O2 is even stronger than the O1···H3−O2 hydrogen bond in the $Fe^{IV}(O\cdots H_2O)$ complex **^{4}8**, as reflected by the O···H distances and the binding energies in these two complexes. Thus, H_2O_2 can be attracted by the ferryl iron more easily than H_2O. In **^{4}12**, the hydroperoxyl group is weakly coordinated to the hydroxyl ligand bound to the iron center.The $Fe^{III}(OH\cdots O_2H)$ complex **^{4}14** is structurally similar to **^{4}12**, but the hydrogen bond between the hydroperoxyl group and the Fe-bound hydroxyl ligand is much stronger in **^{4}14** than in **^{4}12**, as seen from their structures. In fact, the BSSE-corrected binding energies between the hydroperoxyl group and the hydroxyl ligand in **^{4}12** and **^{4}14** are 2.2 and 9.8 kcal/mol, respectively. Thus, the free hydroperoxyl radical generated from **^{4}12** could be easily "trapped" by **^{3}13** to form a more stable species **^{4}14**.

In **^{4}15ts**, the transferred hydrogen atom is almost on the middle way between two neighboring oxygen atoms. In the $Fe^{II}(H_2O\cdots O_2)$ complex **^{4}16**, the O2−O3 bond length is almost the same as that in free $^3O_2$, and the large O3−H5 distance (2.15 Å) means that the oxygen molecule is ready to leave. The $Fe^{II}(H_2O\cdots O_2)$ complex **^{6}16** is structurally analogous to **^{4}16**, but its Fe−O bond is somewhat longer than that in **^{4}16**.

3.4. Spin Densities and Electronic Structures for Species at the Quartet State. The spin densities on atoms of all species are listed in Table 2. For the O−O bond cleavage step from the $Fe^{II}(H_2O_2)$ species **^{4}2** to the $Fe^{III}(OH\cdots OH)$ complex **^{4}4**, the spin densities on the O1 and O2 atoms change from (0.02, 0.0) to (0.29, −0.90) and the total natural charge on the O1−H3 and O2−H4 fragments changes from (0.01, 0.04) to (−0.39, −0.09). These results show that the formed O2−H4 is a radical. Thus, this step is an O−O bond homolytic dissociation.

In the step from the $Fe^{III}(OH\cdots OH)$ species ^{4}**6** to $Fe^{IV}(O\cdots H_2O)$ complex ^{4}**8**, the natural charge on H3 remains almost unchanged and the spin density on the O2−H4 fragment decreases from 1.01 to 0.0. Clearly, this step is a hydrogen atom transfer process and not a proton-transfer process.

The $Fe^{III}(OH)$ species ^{3}**5** and ^{3}**13** are chemically identical, with the same stoichiometry, charge, and spin state, although their structures are slightly different. This geometrical difference leads to different electronic configurations for ^{3}**5** and ^{3}**13**, as seen from their spin distributions in Table 2.

In the $Fe^{II}(OH\cdots OH)$ complexes ^{4}**6**, the spin distribution is very similar to that in ^{3}**5**, in which an unpaired electron in the annulene is antiparallel to two unpaired electrons on the iron. We also found another quartet state of the $Fe^{II}(OH\cdots OH)$ species with an unpaired electron in the annulene ferromagnetically coupled to the unpaired electrons on the iron. However, its energy is 5.5 kcal/mol higher than that of ^{4}**6**.

The spin density on the annulene ring of all species from ^{4}**2** to ^{4}**8** indicates that there always exists an unpaired electron in the macrocycle ligand in stage 1. This result suggests that the annulene ring does not provide electrons in the reaction of stage 1. Hence, the electrons for the oxygen reduction in stage 1 are from the iron center. Comparing compound I in catalases and the $Fe^{IV}O$ intermediate ^{4}**9** obtained here, we note that in compound I the porphyrin ligand is able to provide an electron for the oxygen reduction, while in the present case both electrons are provided by the iron atom. However, since the annulene ring has been oxidized in the resting state of the catalyst, one electron in fact formally originates from the annulene ring.

In the oxoferryl species ^{4}**9**, the spin densities on iron and oxygen are 1.28 and 0.90, respectively, while the spin density on the macrocycle is 0.82. This result indicates that there are two α electrons in Fe−O π^* orbitals and a α electron in the annulene macrocycle ligand, which is similar to the molecular orbital picture describing the electronic state of compound I [49,50] The oxidation state of iron in ^{4}**9** is likely to be Fe(IV), as in the compound I in native catalases.

From the $Fe^{IV}(O\cdots H_2O_2)$ complex ^{4}**10** to the $Fe^{III}(OH\cdots O_2H)$ species ^{4}**12**, the spin densities on the O1 atom and the O2−O3−H5 fragment vary from (0.76, 0.01) to (0.09, 1.02), respectively. Thus, the O2−O3−H5 fragment in ^{4}**12** is a hydroperoxyl radical. This step is clearly a hydrogen atom transfer process. The structure of ^{3}**13** is very close to that of the Fe−OH moiety of ^{4}**12**, and the spin density on the iron center in ^{3}**13** is close to that in ^{4}**12**.

From the $Fe^{III}(OH\cdots O_2H)$ species ^{4}**14** to the $Fe^{II}(H_2O\cdots O_2)$ complex ^{4}**16**, the spin density on iron decreases from 1.26 to 0.02 and the spin density on the O2−O3 fragment increases from 1.01 to 1.99. So the hydrogen atom is transferred from the O2−O3−H5 fragment to O1 and the iron atom is reduced. The spin population in ^{4}**16** clearly shows that there is only an unpaired electron in the annulene ligand and the O2−O3 group is in the triplet state. The difference between electronic configurations of ^{4}**16** and ^{6}**16** is that the iron atom is in the triplet state in ^{6}**16** but in the singlet state in ^{4}**16**. The spin population in ^{6}**16** clearly shows that the removal of H_2O and O_2 would recover the catalyst ^{4}**1**.

3.5. Comparisons with Experimental Results and Related Theoretical Studies. Under the experimental conditions, the catalytic reaction proceeds at room temperature, and the apparent rate constant ($k_{app} = k_{cat}/K_m$) is about 1.5×10^3 M^{-1} s^{-1}. Since the value of K_m (Michaelis constant) was only estimated to be larger than 1.0 M in the experiments,[25] one can infer that the catalytic constant k_{cat} should not be less than 1.5×10^3 s^{-1}. According to our calculations, the free energy barrier for the rate-determining step with the bulk solvent effect included is about 10.7 kcal/mol. This barrier corresponds to 8.9×10^4 s^{-1} for the rate-determining step according to transition state theory. Thus, the mechanism we proposed for the studied reaction is reasonably consistent with the experimental facts.

According to our proposed mechanism, hydroxyl and hydroperoxyl radicals are formed in reaction processes, which may lead to the occurrence of side reactions. This is also in accord with the experimental facts that free hydroxyl radicals were detected in the reaction.[25] Since the generated hydroxyl radicals oxidize the annulene ligand of the catalyst, the catalyst is deactivated after a turnover of about 79 mol of hydrogen peroxide/mol of catalyst.[25] This fact is also in agreement with our calculations that the formed radicals can be effectively quenched in strongly exothermic steps. In recent DFT investigations on the mechanism of manganese catalase, a similar mechanism for the O−O bond homolytic cleavage was reported.[15] The formed hydroxyl radicals can also be efficiently quenched to keep the high activity of manganese catalase.

It is also interesting to compare our results on the O−O bond cleavage with those from experimental and other theoretical studies.[17,51−56] In free H_2O_2, our calculations show that the O−O homolytic cleavage requires 54.2 kcal/mol, which is significantly larger than the electronic energy barrier of 10.8 kcal/mol (from ^{4}**2** to ^{4}**4**) we obtained in this study. An alternative way to break the O−O bond of H_2O_2 is that a proton first transfers from one oxygen to another oxygen atom, and then the O−O bond is heterolytically broken to form water and oxygen atom. The first proton-transfer step was calculated to has a very high barrier of 57.1 kcal/mol, and the second step involves a barrier of 30.6 kcal/mol.[56] The O−O cleavages of H_2O_2 assisted by metal ions such as

(49) Yoshizawa, K.; Shiota, Y.; Yamabe, T. *J. Am. Chem. Soc.* **1998**, *120*, 564.
(50) Shaik, S.; Filatov, M.; Schröder, D.; Schwarz, H. *Chem.—Eur. J.* **1998**, *4*, 193.
(51) Nam, W.; Han, H.-J.; Oh, S.-Y.; Lee, Y.-J.; Choi, M.-H.; Han, S.-Y.; Kim, C.; Woo, S. K.; Shin, W. *J. Am. Chem. Soc.* **2000**, *122*, 8677.
(52) Rodríguez-López, J. N.; Lowe, D. J.; Hernández-Ruiz, J.; Hiner, A. N. P.; García-Cánovas, F.; Thorneley, R. N. F. *J. Am. Chem. Soc.* **2001**, *123*, 11838.
(53) Hiner, A. N. P.; Raven, E. L.; Thorneley, R. N. F.; García-Cánovas, F.; Rodríguez-López, J. N. *J. Inorg. Biochem.* **2002**, *91*, 27.
(54) Filizola, M.; Loew, G. H. *J. Am. Chem. Soc.* **2000**, *122*, 18.
(55) Meredith, C.; Hamilton, T. P.; Schaefer, H. F., III. *J. Phys. Chem.* **1992**, *96*, 9250.
(56) Woon, D. E.; Loew, G. H. *J. Phys. Chem. A* **1998**, *102*, 10380.

Fe^{3+} and Mg^{2+} have also been investigated theoretically.[56] Calculations showed that with the assistance of metal ions the proton-transfer barrier could be reduced to some extent but is still quite high. Recently, Baerends' group has carried out extensive calculations to investigate the mechanism of hydrogen peroxide with a $[Fe^{II}(H_2O)_6]^{2+}$ complex.[31a,e] The mechainsm we obtained here for the studied catalase model is very similar to that obtained by them. For example, the reaction catalyzed by the $[Fe^{II}(H_2O)_6]^{2+}$ complex also consists of two stages, with the Fe(IV)−oxo species as the key intermediate, being in contrast to the widely accepted mechanism[29] that a free hydroxyl radical is the key intermediate. For this reaction, the first stage also proceeds along the O−O bond homolytic cleavage path rather than the proton-transfer path. Especially, the energy barrier of this O−O bond breaking is calculated to be about 6 kcal/mol, close to the value 10.8 kcal/mol we obtained here. The mechanism for the O_2 evolution stage of this reaction is also almost parallel to the mechanism we obtained for the current model. However, the mechanism of quenching the generated OH radicals in the reaction processes is different for the $[Fe^{II}(H_2O)_6]^{2+}$ species and the Ann−Fe(III) complex. For the ferrous ion in water, once the OH radical forms through an O−O homolytic cleavage from the reactant $[Fe^{II}(H_2O)_5(H_2O_2)]^{2+}$, it can abstract a hydrogen from the neighboring water ligand to form a new water molecule (an intermediate $[Fe^{IV}(H_2O)_4(OH)_2]^{2+}$ is simultaneously formed). While, for the current model, the OH radical has to rotate so that its oxygen can approach the hydrogen of the Fe-bound OH ligand to form an intermediate $Fe^{III}(OH\cdots OH)$ (**^{4}6**).

For heme peroxidases, two mechanisms for breaking the O−O bond were proposed.[53] In the heterolytic mechanism, the first step is that the distal histidine (His42) abstracts a proton from hydrogen peroxide. Then the proton is donated back from the histidine to the other oxygen of the peroxide, and simultaneously the O−O bond is heterolytically broken, forming water and compound I. The DFT calculated barrier is 10.4 kcal/mol.[17] In the homolytic mechanism, a proton is first released to form an Fe−OOH species. Then the O−O bond breaks homolytically to form a hydroxyl radical and compound I.[53] In the molecular dynamics simulations of horseradish peroxidase, two possible mechanisms, which are both heterolytic, were suggested when the distal histidine is in a neutral or cationic form.[54] For the studied reaction, we also investigated the proton transfer pathway that is the first step of both mechanisms mentioned above for the heme peroxidases. Our results as described previously show that under the experimental conditions the water solvent is unlikely to play an important role in assisting the O−O bond breaking in the studied reaction.

Apparently, the picture of the O−O cleavage in the catalase model we study is quite different from that in the heme peroxidases and heme catalases. In the present case, the coordination of hydrogen peroxide to the iron center of the catalyst **1** makes the O−O homolytic cleavage occur directly without first releasing a proton. The main reason for accounting for this difference may be that the resting state of the present ferric catalyst in fact consists of a ferrous iron plus a "cation-radical" ligand, but most of heme peroxidases and heme catalases feature a ferric resting state. Thus, this work reveals an exciting hybrid of ferrous−peroxo and ferric−peroxo chemisty, as also supported by recent theoretical calculations on some ferrous− and ferric−hydroperoxo heme models.[57]

4. Conclusions

DFT calculations have been performed to investigate the mechanism of the H_2O_2 dismutation catalyzed by the Ann−Fe(III) complex. From our study, the rate-determining step in the H_2O_2 dismutation by this complex is found to be the O−O bond homolytic cleavage. This step has a calculated free energy barrier of 10.8 kcal/mol at the quartet state, which is in reasonable agreement with the experimental facts. The O−O bond homolytic cleavage, without the assistance of additional water molecules in the second coordination shell, is an important finding of this study, which is different from those suggested in H_2O_2 dismutation reactions catalyzed by heme peroxidases and heme catalases.

Another interesting part of the mechanism suggested here for the catalytic cycle of the Ann−Fe(III) complex is that the hydroxyl and hydroperoxyl radicals are generated in the reaction processes. However, our calculations show that the hydroxyl and hydroperoxyl radicals can be efficiently quenched in strongly exothermic steps.

In summary, the calculated low free energy barrier for the rate-determining step and the facile quenching of the generated hydroxyl and hydroperoxyl radicals provide a satisfactory explanation to the observed efficiency of the H_2O_2 dismutation catalyzed by the Ann−Fe(III) complex.

Acknowledgment. Parts of the calculations were carried out on SGI Origin 3800 and 3000 instruments at Nanjing University. This work was supported by the National Natural Science Foundation of China (Grant No. 20373022 and 20233020). We are grateful to the reviewers for their pertinent comments and good suggestions concerning our original manuscript.

Supporting Information Available: Tables of electronic energies and atomic coordinates for optimized structures, figures of crystal, optimized, and model structures, and text discussing model systems. This material is available free of charge via the Internet at http://pubs.acs.org.

IC049715J

(57) Silaghi-Dumitrescu, R. *Arch. Biochem. Biophys.* **2004**, *424*, 137.